Chemistry & Biology, Vol. 12, 427–437, April, 2005, ©2005 Elsevier Ltd All rights reserved. DOI 10.1016/j.chembiol.2005.01.016

Mirror-Image Packing in Enantiomer Discrimination: Molecular Basis for the Enantioselectivity of *B. cepacia* Lipase toward 2-Methyl-3-Phenyl-1-Propanol

Alessandra Mezzetti,[1,3] Joseph D. Schrag,[2] Chan Seong Cheong,[1,4] and Romas J. Kazlauskas[1,5,*]
[1]Department of Chemistry
McGill University
801 Sherbrooke Street West
Montréal, Québec, H3A 2K6
Canada
[2]Biotechnology Research Institute
National Research Council of Canada
6100 Royalmount Avenue
Montréal, Québec, H4P 2R2
Canada

Summary

Synthetic chemists often exploit the high enantioselectivity of lipases to prepare pure enantiomers of primary alcohols, but the molecular basis for this enantioselectivity is unknown. The crystal structures of two phosphonate transition-state analogs bound to *Burkholderia cepacia* lipase reveal this molecular basis for a typical primary alcohol: 2-methyl-3-phenyl-1-propanol. The enantiomeric alcohol moieties adopt surprisingly similar orientations, with only subtle differences that make it difficult to predict how to alter enantioselectivity. These structures, along with a survey of previous structures of enzyme bound enantiomers, reveal that binding of enantiomers does not involve an exchange of two substituent positions as most researchers assumed. Instead, the enantiomers adopt mirror-image packing, where three of the four substituents at the stereocenter lie in similar positions. The fourth substituent, hydrogen, points in opposite directions.

Introduction

Molecular recognition, especially enantiomer recognition, is a key to the biological specificity of many current drugs. Enantiopure compounds for pharmaceutical intermediates and other uses is currently a rapidly growing multibillion business worldwide [1]. Understanding enantiomer recognition is key to both understanding the mechanism of action of these drugs and to designing good synthetic routes to enantiopure compounds. Unfortunately, our understanding of enantiomer recognition is still primitive and most drug design and synthesis design rely on trial and error. In this paper, we identify the molecular basis of enantiomer recognition of a lipase toward an unnatural substrate.

Lipases show moderate to high enantioselectivity toward a wide range of primary and secondary alcohols, making them useful catalysts for the preparation of these important building blocks for chiral drugs. For example, a primary alcohol, (*R*)- and (*S*)-2-methyl-3-phenyl-1-propanol ([MPP], Figure 1A), is a precursor for fungicidal compounds [2], adenosine receptor agonists and antagonists [3], and a cholesterol biosynthesis inhibitor [4]. Although many lipases show high enantioselectivity toward secondary alcohols, only a few—*Burkholderia cepacia* lipase (BCL, formerly called *Pseudomonas cepacia* lipase), porcine pancreatic lipase, and *Achromobacter sp.* lipase—also show high enantioselectivity toward primary alcohols [5, 6]. The molecular basis for this enantioselectivity toward primary alcohols is uncertain. Understanding it would allow rational design of substrates (substrate engineering), reaction conditions (medium engineering), and enzyme (protein engineering) for higher enantioselectivity.

Lipases are serine hydrolases and lipase-catalyzed ester hydrolysis involves two successive tetrahedral intermediates. The first tetrahedral intermediate, T_d1, releases the alcohol and forms the acyl enzyme (Figure 1B), while the second tetrahedral intermediate, T_d2, releases the acid. Only T_d1 includes the alcohol moiety and therefore only T_d1 contributes to enantioselectivity (*E*) of lipases toward chiral alcohols.

Previous molecular modeling of this tetrahedral intermediate [7, 8], a similar one [9], or phosphonate analogs in the active site of BCL suggested several possible origins of enantioselectivity toward primary alcohols. The modeling focused on the hydrolysis of the acetate or butanoate ester of a typical primary alcohol, 2-methyl-3-phenyl-1-propanol (MPP) [7, 8]. Two research groups suggested that the relative orientation of the enantiomers involves an exchange of positions of the methyl and hydrogen substituents (Figure 2). However, the orientation of the primary alcohol moiety and the proposed explanation for enantioselectivity differed. Tuomi and Kazlauskas [7] suggested that enantioselectivity stems from a better binding of the fast-reacting enantiomer. Zuegg et al. [9] proposed a similar explanation for 2-phenyl-1-butanol, a similar primary alcohol containing one more CH_2 group. However, Tomić et al. [8] suggested that enantioselectivity stems from a shorter key hydrogen bond between the catalytic serine and histidine.

Here we report an experimental approach to identify the origin of enantioselectivity using X-ray crystal structures of transition state analogs bound to BCL. These structures contain the same alcohol moiety as the modeling above, but different acyl groups. The modeling used the acetate or butanoate esters, while the X-ray structures mimic reaction of the heptanoate ester. The relative orientations of the enantiomers in these structures differ significantly from the modeling.

*Correspondence: rjk@umn.edu
[3]Present address: Biotechnology Research Institute, National Research Council of Canada, 6100 Royalmount Avenue, Montréal, Québec, H4P 2R2, Canada.
[4]Present address: Life Sciences Division, Korea Institute of Science and Technology, Cheongryang 131, Seoul 130-650, South Korea.
[5]Current address: Department of Biochemistry, Molecular Biology, and Biophysics and The Biotechnology Institute, University of Minnesota, 1479 Gortner Avenue, St. Paul, Minnesota 55108.

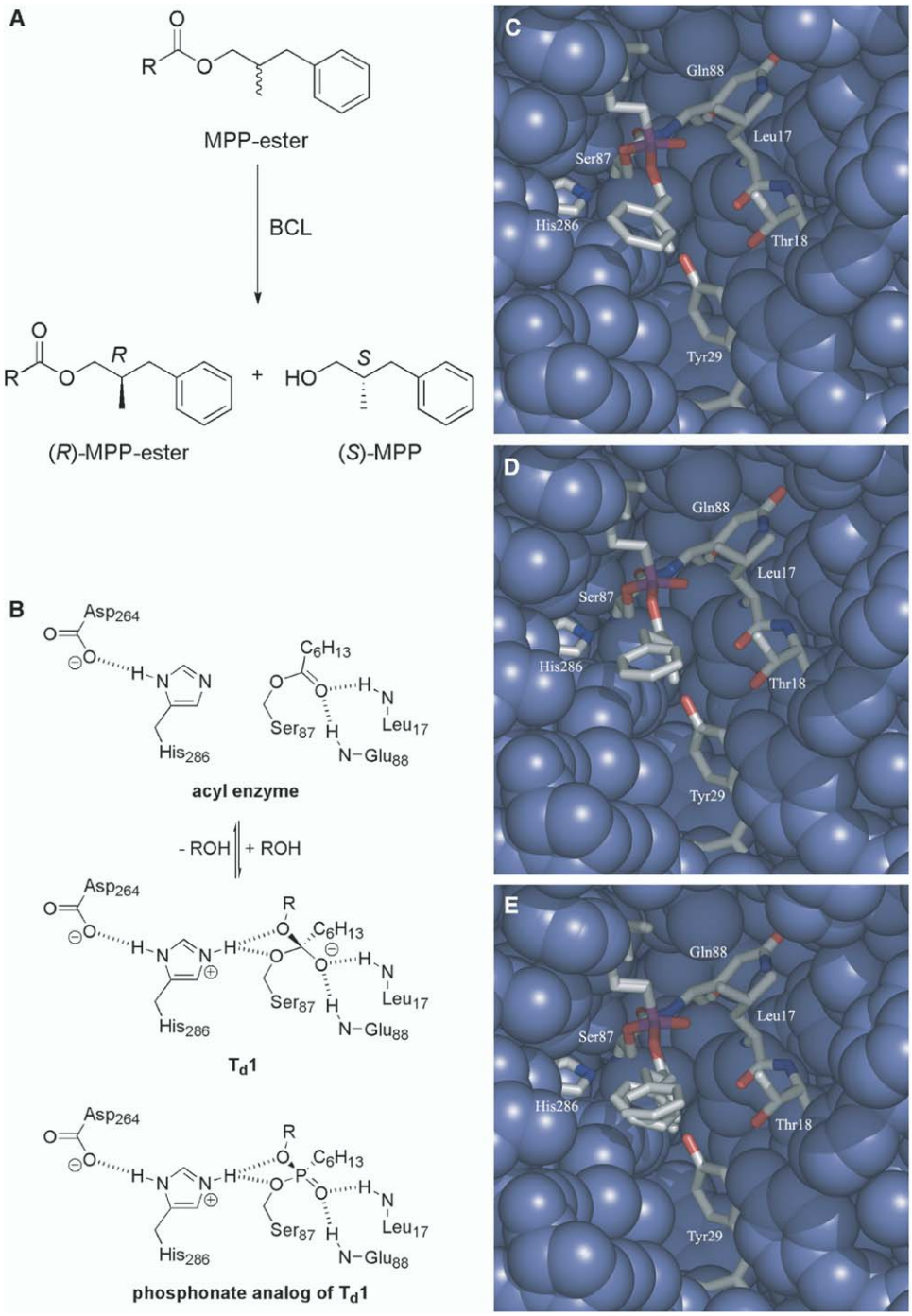

Figure 1. Phosphonates Mimic the Transition State in the BCL-Catalyzed Resolution of MPP Esters

On the left, from the top: (A) BCL catalyzed hydrolysis of racemic MPP-ester yields (*R*)-MPP-ester and (*S*)-MPP. (B) The first tetrahedral intermediate T_d1 releases alcohol (ROH) to form an acyl enzyme in the BCL-catalyzed hydrolysis of esters. The formation and/or breakdown of this tetrahedral intermediate determines the enantioselectivity of BCL toward alcohols. The phosphonate analog mimics T_d1. On the right, from the top: BCL-inactivator complexes. (C) BCL-1-(*R*), (D) BCL-1-(*S*), (E) overlay of BCL-1-(*R*) and BCL-1-(*S*). In (C), (D), and (E), catalytic triad residues His286 and Ser87, oxyanion hole residues Glu88 and Leu17, nearby residues Thr18, Tyr29, and Leu287 and phosphonate esters are in stick representation.

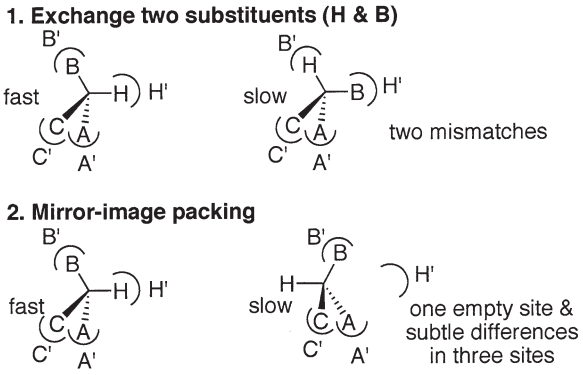

Figure 2. Enantiomer Recognition by Enzymes Relies on Interactions between the Substituents at the Stereocenter and the Recognition Site

For the fast-reacting enantiomer all four interactions match. For the slow-reacting enantiomer, only two substituents match when all the substituents point to the interaction sites. (Exchanging substituents H and B of the fast enantiomer creates the slow enantiomer.) However, if one substituent of the slow enantiomer does not interact with any of the four sites, then the three remaining substituents match. (An umbrella-like inversion of the fast enantiomer stereocenter along the C–H bond creates slow enantiomer). X-ray crystal structures of enantiomeric configuration bound to enzyme suggest the second mechanism is the most common one.

Results

Synthesis of Phosphonate Esters and Inhibition of BCL

A straightforward modification of published procedures [10, 11] yielded two phosphonate *p*-nitrophenyl esters that contain as alcohol moieties pure enantiomers of (*R*)-MPP or (*S*)-MPP (Table 1). While phosphonyl chlorides containing secondary alcohol moieties are relatively stable [10, 11], these phosphonyl chlorides contained primary alcohols and were not stable. We therefore replaced the chloride leaving group with the less reactive *p*-nitrophenol. Nucleophilic displacement of one chloride of hexylphosphonic dichloride by one equivalent of chiral alcohol yielded a mono-substituted phosphonyl chloride, which was converted in situ to the desired *p*-nitrophenyl derivative by treatment with two equivalents of *p*-nitrophenol in the presence of di-isopropyl ethylamine. Each reaction formed an equimolar mixture of (S_P) and (R_P) epimers due to the phosphorous stereocentre (^{31}P NMR showed two resonances for the phosphorous atom (see Experimental Procedures). We did not attempt to separate the epimers.

Inactivation of BCL with 1000-fold excess of either 1-(*R*) or 1-(*S*) irreversibly inhibited more than 98% of the hydrolytic activity of BCL toward *p*-nitrophenol acetate. The solvent for the inactivation of BCL was 50 vol% *n*-propanol in aqueous buffer because the BCL-inactivator complexes precipitated from buffer containing less than 50 vol% *n*-propanol.

Crystal Structure of BCL-Inactivator Complexes

We crystallized the BCL-inactivator complexes by the hanging drop method using a reservoir containing 25% *n*-propanol in imidazole buffer 50 mM (pH 6.5). We estimate that the crystals formed at a concentration of *n*-propanol of about 30%. The crystals of the inhibited complexes were isomorphous with the crystals of the open form of BCL previously reported (PDB ID 3LIP [12]). Similarly, the X-ray structures of the complexes show no significant differences in the polypeptide backbone or in the side chain conformations compared with the open conformation of BCL. The root mean squared deviation (rmsd) in Cα positions between the open form of BCL and the BCL-1-(*R*) and BCL-1-(*S*) complexes are 0.41 Å and 0.39 Å, respectively. Data collection and refinement statistics (Table 1) show that the structures are of high quality with resolutions of 1.10 and 1.50 Å.

Both phosphonate esters bind similarly to BCL (Figures 1C–1E). Both covalently link the phosphorous to Oγ of catalytic Ser87 and have R_P configuration. Nucleophilic attack at phosphorus by Oγ of the catalytic serine likely proceeds with inversion of configuration at phosphorus [13]; thus, the favored epimer had S_P configuration prior to the reaction. The hexyl chain of the phosphonate esters extends into the hydrophobic groove HA (Figures 1C–1E). Lang et al. [14] reported similar acyl chain orientation for a triacylglycerol analog bound to BCL. In both BCL-1-(*R*) and BCL-1-(*S*), the phosphonate esters fold into a hairpin with similar distances between the hexyl chain and the benzylic CH_2 (4.9 Å in BCL-1-(*R*) and 5.3 Å in BCL-1-(*S*)). All distances refer to heavy atom to heavy atom distances (e.g., between carbons of two methylene groups) unless specified otherwise. The superimposed structures show that the alcohol oxygen O_l, the medium substituent (CH_3), and the large substituent ($PhCH_2$) all lie in a similar position in BCL-1-(*R*) and in BCL-1-(*S*). The alcohol oxygens O_l differ by only 0.3 Å. Surprisingly, the large substituents ($PhCH_2$) lie in a solvent-exposed crevice (Figures 1C–1E) and are not bound to hydrophobic regions of the substrate binding site. Since three substituents at the stereocenter are in similar positions, the fourth hydrogen must differ to account for the enantiomeric configurations at the carbon stereocenter. Indeed the hydrogen substituents of the two structures point in opposite directions. Thus, the alcohol portions of BCL-1-(*R*) and BCL-1-(*S*) adopt a mirror-image orientation, Figure 2.

Both inactivators mimic a catalytically productive orientation because they contain all the five hydrogen bonds necessary for catalysis (Table 2). The phosphonyl oxygen in the oxyanion hole is hydrogen bonded to the NH of Leu17 and Glu88 (2.73 Å and 2.81 Å in BCL-1-(*R*); 2.73 Å and 2.82 Å in BCL-1-(*S*)). The catalytic Ser87 Oγ is hydrogen bonded to His286 Nε2 (3.05 Å, 116° in BCL-1-(*R*); 3.02 Å, 115° in BCL-1-(*S*)). These hydrogen bond angles are slightly more acute than the 180°–120° expected for a hydrogen bond. The catalytic Asp264 Oδ2 is at hydrogen bonding distance from His286 Nδ2 (2.81 Å in BCL-1-(*R*); 2.82 Å in BCL-1-(*S*)). The oxygen O_l of the alcohol moiety forms a similar hydrogen bond with His286 Nε2 in both structures (3.30 Å, 126° in BCL-1-(*R*); 3.17 Å, 132° in BCL-1-(*S*)).

Both inactivators have a *gauche*$^+$ conformation between the Ser87 Oγ-P bond and the O_l-CH_2 bond of the

Table 1. Data Collection Statistics and Refinement Parameters

Phosphonate Inactivators	BCL-1-(*R*) 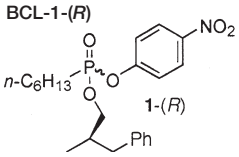 1-(*R*)	BCL-1-(*S*) 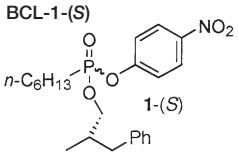 1-(*S*)
Data statistics		
Resolution range (Å)	44.4–1.10	37.8–1.50
Highest resolution shell (Å)	1.14–1.10	1.55–1.50
Space group	C2	C2
Unit cell dimensions		
a (Å)	88.8	88.9
b (Å)	46.2	46.2
c (Å)	84.6	84.7
(°)	90	90
β (°)	121.3	121.3
γ (°)	90	90
Mosaicity (°)	0.22	0.27
R merge (%)	4.1 (10.6)	4.3 (12.7)
Completeness of the data (%)	89.2 (40.8)	90.3 (53.5)
No. of observations	495813	152333
No. of unique reflections	105990	42707
Mean I/σI	21.0 (4.6)	19.0 (5.4)
Refinement statistics		
Total non-hydrogen atoms	2498	2498
Protein atoms	2331	2331
No. of waters	147	147
No. of calcium ions	1	1
Final R factor (%)[a]	16.0	16.7
Final R free (%)[b]	17.2	18.1
Rms deviations from ideality for		
Bond lengths (Å)	0.008	0.014
Bond angles (°)	1.38	1.47
Mean B factors (Å^2)		
Protein	8.47	9.01
Solvent	13.15	13.89
Calcium ion	6.39	6.66
Inactivator	12.17	10.42

[a] R factor = $\Sigma F_c - F_o/\Sigma F_o \times 100$ where F_c and F_o are the calculated and observed structure factor amplitudes.
[b] 5% of the total reflections were randomly selected and used to calculate R free.

alcohol moiety (dihedral angle Ser87Oγ-P-O_l-CH_2 of 72° in BCL-1-(*R*) and of 77° in BCL-1-(*S*)). In the true tetrahedral intermediate, this orientation may promote release of Ser87 Oγ and the return to the starting esters due to overlap between the lone pair of the alcohol oxygen and the σ* orbital of the Oγ-P bond [15]. Since both transition state analogs adopt this orientation, it cannot contribute to the enantioselectivity.

The most striking difference is the position of the hydrogen, which points in opposite directions in the two enantiomers. Neither orientation makes significant interactions with the enzyme. In BCL-1-(*S*) the hydrogen at the stereocenter is at 3.68 Å from His298 Cδ2 while in BCL-1-(*R*) it is at 3.25 Å from Leu17 carbonyl oxygen (Table 2).

The CH_2(1)-O_l substituent orientation differs little in the two structures. As mentioned above, the hydrogen bond to His286 Nε2 is nearly identical. Other, barely significant differences are that CH_2(1) in BCL-1-(*S*) is slightly closer to Leu17 carbonyl (3.50 Å versus 3.60 Å) and to His86 Cε1 (4.24 Å versus 4.41 Å) (Table 2).

The benzylic CH_2(3) shows only subtle differences in the two structures (Table 2). For the faster reacting BCL-1-(*S*) it lies close to the carbonyl oxygen of Leu17 (3.52 Å). This interaction may be unfavorable because Schultz et al. [16] suggested that atoms other than hydrogen cause repulsion when directed toward this residue. For the slow (*R*)-enantiomer, CH_2(3) is close to catalytic His286 (4.07 Å to Nε2, 3.77 Å to Cδ2, and 3.87 Å to Cγ of His286), which may also cause steric strain.

The phenyl shows a more favorable interaction with BCL for the fast-reacting (*S*)-enantiomer (Table 2). The phenyl ring of (*S*)-MPP is slightly closer to the side chain methyl groups of Leu287 (mean distance of 4.43 Å in (*S*)-MPP versus 4.72 in (*R*)-MPP), suggesting better hydrophobic interaction for the fast-reacting (*S*)-enantiomer. On the other hand the phenyl ring of (*R*)-MPP is closer to Cγ1 of Thr18 (mean distance of 5.17 Å versus 5.42 Å), but this distance is too long for a significant interaction. The phenyl ring of slow-reacting (*R*)-MPP shows two different orientations (dihedral angle CH_3-C*-CH_2-Ph 48° versus 70°) suggesting that it binds less tightly than (S)-MPP, which shows only one orientation.

The methyl substituent shows similar positions (only 0.63 Å apart) in BCL-1-(*S*) and BCL-1-(*R*). One interac-

Table 2. Key Hydrogen Bond Distances (Heavy Atom to Heavy Atom) and Key Angles in the Two BCL-Inactivator Complexes and Summary of Subtle Interactions Alcohol Moiety-Enzyme Residues that May Contribute to the Enantioselectivity in the Complexes BCL-Inactivator

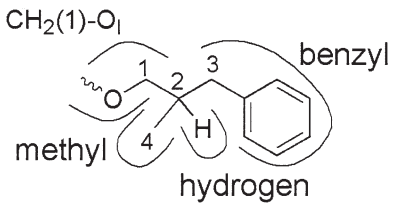

Key Hydrogen Bond Distances	BCL-1-(*R*)	BCL-1-(*S*)
Leu17 N(H)–O=P, Å[a]	2.73	2.73
Gln88 N(H)–O=P, Å[a]	2.81	2.82
Nδ2 His286–Oδ2 Asp264, Å	2.81	2.82
Nϵ2 His286–Oγ Ser87, Å	3.05	3.02
His286 Nϵ2–H–Oγ Ser87 θ, °	116	115
Nϵ2 His286–O_I[b], Å	3.30	3.17
His286 Nϵ2–H–O_I[b], θ, °	126	132
Ser87Oγ–P–O_I–CH_2, θ, °	72	77
Interactions	**BCL-1-(*R*)**	**BCL-1-(*S*)**
Benzyl substituent		
Leu287 s.c.[c]–Ph	mean 4.72 Å	mean 4.43 Å
Thr18 Cγ1–Ph	mean 5.17 Å	mean 5.42 Å
His286 s.c.[c]–CH_2(3)	4.07 Å to Nϵ2	—[d]
	3.77 Å to Cδ2	—[d]
	3.87 Å to Cγ	—[d]
Leu17 C=O–CH_2(3)	—[d]	3.52 Å
CH_2(1)-O_I substituent		
Leu17 C=O–CH_2(1)	3.60 Å	3.50 Å
His286 Nϵ2–O_I	3.30 Å, 126°	3.17 Å, 132°
His86 s.c.–CH_2(1)	4.41 Å to Cϵ1	4.24 Å to Cϵ1
	5.36 Å to Nϵ2	5.23 Å to Nϵ2
	4.64 Å to Nδ1	4.41 Å to Nδ1
Hydrogen substituent		
Leu17 C=O–CH(2)	3.25 Å	—[d]
His286 Cδ2–CH(2)	—[d]	3.68 Å
Methyl substituent		
Thr 18 Cγ1–CH_3(4)	4.81 Å	5.37 Å
Thr 18 Oγ1–CH_3(4)	3.79 Å	4.06 Å
Leu17 C=O–CH_3(4)	3.37 Å	3.62 Å
Tyr29OH–CH_3(4)	4.11 Å	3.62 Å
His86 s.c.–CH_3(4)	4.85 Å to Cϵ1	4.32 Å to Cϵ1
	6.03 Å to Nϵ2	5.54 Å to Nϵ2
	5.19 Å to Nδ1	4.61 Å to Nδ1

[a] The angles N-H-O range from 164° to 166°, which is typical of hydrogen bonds.
[b] O_I is the MPP alcohol oxygen.
[c] s.c. = side chain.
[d] —, too far away for significant interaction.

tion is more crowded for the fast-reacting enantiomer. The methyl substituent of BCL-1-(*S*) lies 3.62 Å from Tyr29 OH, while in BCL-1-(*R*) it is 4.11 Å away. Two other interactions are more crowded for the slow-reacting enantiomer. The methyl substituent of BCL-1-(*R*) lies 3.79 Å from Oγ1 of Thr18, while in BCL-1-(*S*) it is 4.06 Å away. The methyl substituent of BCL-1-(*R*) lies 3.37 Å from the carbonyl oxygen of Leu17, while in BCL-1-(*S*) it is 3.62 Å away.

Enantioselectivity and Kinetic Constants

BCL shows high enantioselectivity ($E \geq 190$) favoring the (*S*)-enantiomer in the hydrolysis of MPP-heptanoate (MPP-C_7) in a solvent similar to that used for crystallization of the BCL-inactivator complexes (Table 3) [17]. (To avoid possible chemical hydrolysis during the enantioselectivity measurement, we replaced the imidazole buffer used for the crystallization of the complexes with phosphate buffer.) The kinetic constants for each enantiomer, determined spectrophotometrically, show similar K_M values for the two enantiomers (3 mM for (*R*)-MPP-C_7 and 4 mM for (*S*)-MPP-C_7), but 100-fold different k_{cat} values (k_{cat} = 0.4 min^{-1} for (*S*)-MPP-C_7 and 0.004 min^{-1} for (*R*)-MPP-C_7) (Table 3). The solubility limit of MPP-heptanoate was approximately equal to K_M, resulting in large standard errors in the measured k_{cat} and K_M values (estimated to be ±25%). Despite this uncertainty, the kinetic constants show that the enan-

Table 3. Kinetic Constants for (*R*) and (*S*)-MPP-C_7

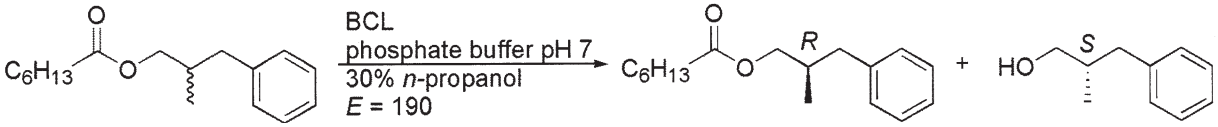

	(R)-MPP-C_7	(S)-MPP-C_7
k_{cat} (min^{-1})	0.004 ± 0.001	0.4 ± 0.1
K_M (mM)	3 ± 1	4 ± 1
(k_{cat}/K_M)	$(1.3 \pm 0.6)10^{-3}$	0.10 ± 0.04
E[a] [(k_{cat}/K_M(S))/(k_{cat}/K_M(R))]	80 ± 50	
End point *E*[b]	>190 ± 30	

Conditions for determination of kinetic constants: [BES] = 7.44 mM, [PNP] = 1.24 mM, [BCL] = 2.85 μg/ml, [(*R*) and (*S*)-MPP-C_7] = 0.6 to 4.5 mM, [*n*-propanol] = 28.8%. Data were analyzed by Eadie-Hofstee plots [27, 28]

[a] Calculated from the k_{cat} and K_M values. This value agrees with the end point E determination within the error limits, providing a check on the determination of the K_M and k_{cat} values.

[b] Determined by GC analysis of reaction products and starting materials at 39% conversion according to Chen et al. [29]. The measured enantiomeric purity of the remaining starting material was 63% ee, while the measured enantiomeric purity of the product was > 98%.

tioselectivity of BCL toward these substrates stems from the higher k_{cat} value with (*S*)-MPP-C_7. Nishizawa et al. [18] reached a similar conclusion from their measured kinetic constants for BCL-catalyzed hydrolysis of similar esters.

Discussion

These X-ray crystal structures of transition state analogs bound to BCL first show that primary and secondary alcohols bind differently to this lipase. The comparison of the X-ray structure of BCL complexed with a phosphonate containing a secondary alcohol moiety ((*R*)-1-phenoxy-2-butanol) [19] with that of BCL-1-(*S*) shows a major difference in the position of the large substituent (Figure 3). The phenoxy group of the secondary alcohol binds in a large hydrophobic pocket (HA pocket), which also binds the acyl moiety of the phosphonates. In contrast, the benzyl group of the primary alcohols points toward the solvent. This binding difference explains why different rules are needed for the enantiopreference of BCL toward primary and toward secondary alcohols [7–9, 20].

The enantiomeric MPP moieties show mirror-image packing. These primary alcohol moieties are flexible since they contain two rotatable bonds between the alcohol oxygen and the stereocenter. However, this flexibility is unlikely to be the only reason for the mirror-image orientation because less flexible moieties also show mirror-image packing. For example, the menthol moiety of CRL-menthol complexes also shows mirror-image packing [10] (Table 4). This secondary alcohol contains only one rotatable bond between the alcohol oxygen and the stereocenter and a six-membered ring, but still shows mirror-image packing. One possible reason for the mirror-image packing is that it allows three substituents to bind in nearly the same position (one mismatch), while exchanging two substituents causes two mismatches, Figure 2. In contrast, molecular modeling always suggests an exchange of two substituents, likely because it mimics the behavior of mechanical models and it is easier to understand. These structures emphasize that modeling enantioselectivity must consider mirror-image packing as a way of making mistakes.

A survey of X-ray crystal structures of enantiomeric ligands bound to enzymes shows that mirror-image packing is the most common way that enantiomers ori-

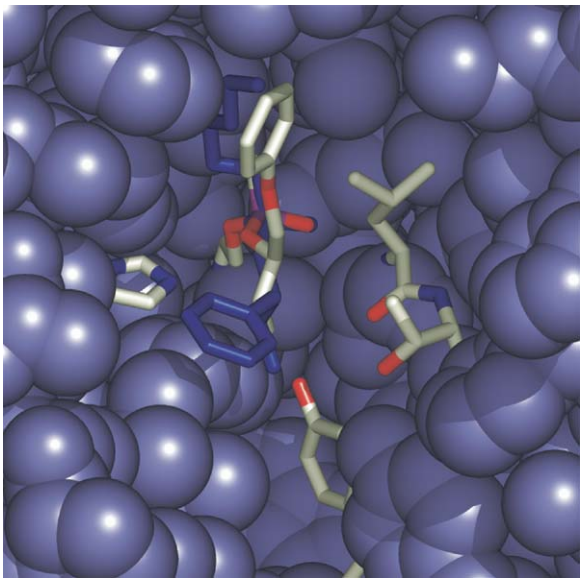

Figure 3. Different Binding of Primary and Secondary Alcohols in BCL

Overlap of stick representations of the BCL complex with *O*-(2*R*)-(1-phenoxy-2-butyl)-methylphosphonyl ([19], [PDB ID 1HQD], cpk colors) with the complex BCL-1-(*S*) (blue). For the secondary alcohol, the large substituent at the stereocenter (phenoxy) binds in a large hydrophobic pocket (upper portion of figure), while for the primary alcohol, the large substituent at the stereocenter (benzyl) points toward the solvent (center of figure). Catalytic triad residues His286 and Ser87, oxyanion hole residue Leu17, residues Thr18 and Tyr29, and inactivators are also in stick representation.

Table 4. Examples of X-Ray Crystal Structures Containing Bound Enantiomeric Ligands

Enzyme	Ligand	Mirror-Image Orientation	PDB Code	Reference
Alanine racemase	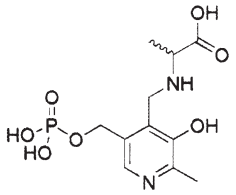	yes, H inverted	1L6F, 1L6G	[30]
Human retinoic acid receptor	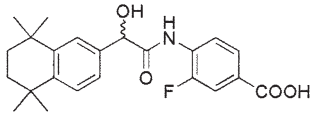	yes, H inverted	1EXA, 1EXX	[31]
Carboxypeptidase A	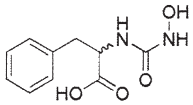	yes, H inverted	1HDQ, 1HEE	[32]
γ-Chymotrypsyn	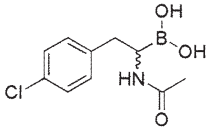	yes, H inverted	1VGC, 2VGC	[33]
γ-Chymotrypsyn	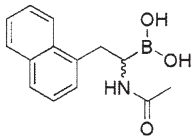	yes, H inverted	3VGC, 4VGC	[33]
Subtilisin Carlsberg	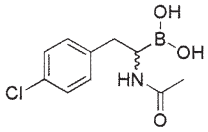	yes, H inverted	1VSB, 1AVT	[33]
Subtilisin Carlsberg	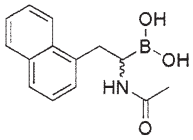	yes, H inverted	1AV7, 3VSB	[33]
Human serum albumin	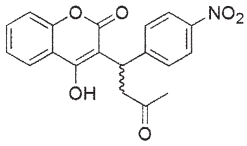	yes, H inverted	1H9Z, 1HA2	[34]
Human methionine aminoipeptidase Type II	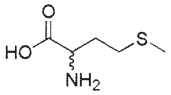	yes, H inverted	1KQ0, 1KQ9	[35]
Herpes simplex type 1 thymidine kinase	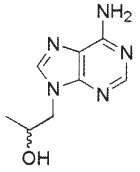	yes, H inverted	1E2I[a]	[36]

(*continued*)

Table 4. Continued

Enzyme	Ligand	Mirror-Image Orientation	PDB Code	Reference
Horse Liver Alcohol Dehydrogenase		yes, H inverted	1BTO, 3BTO	[37]
Candida rugosa lipase	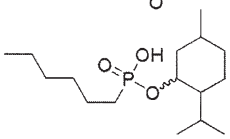	yes, H inverted	1LPM, 1LPS	[10]
Isocitrate dehydrogenase	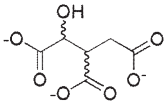	yes, H inverted	1PB1, 1P8F	[38]
Citrate synthase	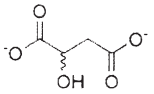	yes, H inverted	3CSC, 4CSC	[39]
Inositol monophosphatase	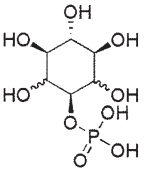	yes, H inverted	1IMA, 1IMB	[40]
Lipoxygenase-3	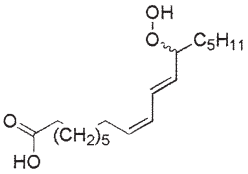	yes, H inverted	1IK3[a]	[41]
Cytochrome P-450$_{CAM}$	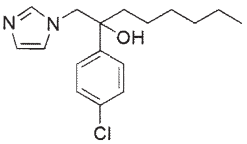	no	1PHA, 1PHB	[42]
Reaction center from *Rodopseudomonas viridis*	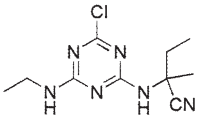	no	6PRC, 7PRC	[43]

In most cases, there are two separate structures for the enantiomers, but in two cases a single crystal structure refined best if the bound ligand was modeled as a mixture of both enantiomers in the same site. One example [44] is not included in the table because the refinement gave flat structure for the sp^3 stereocenter. However, it appears to be an example mirror-image inversion. Another example [45] was not included because the coordinates are not available in the protein data bank, but the figures suggest that it is a mirror-image inversion.
[a]The structure was refined with a mixture of enantiomers in the same site.

ent in proteins (Table 4). In all but two of the eighteen examples a hydrogen adopts a mirror-image orientation in the two enantiomers. The two exceptions contain a quaternary stereocenter, which lacks a hydrogen at the stereocenter. This survey suggests that a C–H lacks significant interactions with protein binding sites and enantiomers containing a hydrogen at the stereocenter favor the mirror-image orientation. Although mirror-image packing of enantiomers was suggested at least 20 years ago [21] and was noted in X-ray structures recently [38], most modeling and discussions only consider exchange of substituents as the orientation of enantiomers.

At first, the two types of experimental data in this paper—phosphonate X-ray structures and kinetic measurements—appear inconsistent. The phosphonate X-ray structures suggest a poorer fit for the slow enantiomer, but the kinetic constants show a similar K_M values for both enantiomers, but 100-fold different k_{cat} values. One way to resolve this contradiction is to hypothesize that the slow enantiomer also binds nonproductively. This nonproductive binding would not

lead to catalysis or a tetrahedral intermediate and thus would not be observed in a phosphonate structure that mimics the tetrahedral intermediate. This nonproductive binding would contribute to a lower K_M since K_M includes both productive and nonproductive binding.

While the nonproductive binding of the slow enantiomer can explain how the kinetic parameters match the X-ray structures, it is not a mechanism of enantiomer recognition. Nonproductive binding lowers both the observed K_M and k_{cat} [22]. The lower K_M comes from the ability of the substrate to bind in another manner; the lower k_{cat} comes from the blocking of the active site by this binding. Selectivity is the ratio of k_{cat} and K_M; thus, this lowering of both kinetic constants does not change selectivity.

Previous lipase-inactivator complexes showed that enantioselectivity toward secondary alcohols stems from a missing key hydrogen bond between the alcohol oxygen and catalytic His Nϵ2 for the slow-reacting enantiomer [10], which could account for the lower k_{cat} of the slow-reacting enantiomer. At present, we cannot exclude either of these explanations for the enantioselectivity and, indeed, both may contribute. Regardless of the exact mechanism it is clear that enantioselectivity stems from subtle differences in the orientations of the two enantiomers.

Given the subtlety of the interactions, it may be difficult to rationally predict substrate modifications or lipase mutations that would increase the enantioselectivity. Indeed, previous substrate modifications to increase the enantioselectivity of BCL toward primary alcohols met with only limited success [20].

Differences between the previous modeling and current phosphonate structures may in part be due to differences in the acyl group. Modeling focused on the acetyl esters, while the phosphonates used here correspond to the heptanoyl esters. The mechanisms of enantioselectivity may differ for the acetate and heptanoate esters of MPP. Enantioselectivity of the BCL-catalyzed hydrolysis of the MPP acetate is at least 10-fold less enantioselective that of MPP heptanoate (E = 16 versus >190 [17]). Further, the enantioselectivity toward MPP acetate stems from differences in K_M [8], while enantioselectivity for MPP heptanoate stems from differences in k_{cat}. The X-ray structures of the phosphonates show that the heptanoyl group binds in the large pocket, but the acetyl group would leave this area free, so that acetate esters of MPP may bind differently.

Significance

Molecular recognition, especially enantiomer recognition, is pivotal to the understanding of the molecular action of enantiopure drugs and critical to the design of new and more efficient synthetic routes to such drugs. Despite this need, our understanding of enantiomer recognition by biological receptors is still primitive and most of the efforts in drug design and synthesis design still rest on trial and error. In this report, we identify the molecular basis for the enantioselectivity of *Burkholderia cepacia* lipase (BCL) toward 2-methyl-3-phenyl-1-propanol (MPP), an unnatural substrate, using X-ray crystal structures of transition state analogs. These X-ray crystal structures reveal a mirror-image packing of enantiomers and only subtle differences between them in spite of a high enantioselectivity of BCL toward these enantiomers. This mirror-image packing allows three substituents at the stereocenter to bind in nearly the same position, while the fourth substituent, hydrogen, points in opposite directions. A survey of other structures of enantiomers bound to enzymes indicates this mirror-image packing is the most common orientation. In contrast, most researchers currently assume that enantiomer recognition involves an exchange of substituent positions. This thinking may stem from mechanical models where interconverting enantiomers requires exchanging two substituents. These assumptions about enantiomer recognition may contribute to the difficulties in understanding enantiomer recognition.

Experimental Procedures

All chemicals were purchased from Sigma-Aldrich Co. (Oakville, ON) unless otherwise specified. Lipase from *Burkholderia cepacia* was purchased from Genzyme Diagnostics (Cambridge, MA) under its older name of *Pseudomonas cepacia* lipase. ^{1}H NMR spectra were collected at 270 MHz, ^{13}C NMR at 68 MHz, and ^{31}P NMR at 109 MHz. Protein images were generated using PyMol [23].

(R_C, R_PS_P) Hexylphosphonic Acid 2-Methyl-3-Phenylpropyl Ester 4-Nitrophenyl Ester, 1-(*R*)

A solution of (*R*)-2-methyl-3-phenyl-propan-1-ol (0.17 g, 1.11 mmol) in dichloromethane (2 ml) was added to a solution of hexylphosphonic dichloride (0.21 ml, 1.11 mmol) and di-isopropyl ethyl amine (0.55 ml, 3.16 mmol) in dichloromethane (9 ml) previously cooled to 5°C with an ice bath. After 1 hr of stirring, 1*H*-tetrazole (0.07 mg, 0.10 mmol) was added. When the (*R*)-2-methyl-3-phenyl-propan-1-ol was consumed (TLC observation, 1.5 hr), the ice bath was removed and an excess of 4-nitrophenol (0.30 g, 2.12 mmol) was added to the reaction mixture. After 3 hr an excess of di-isopropyl ethyl amine (0.40 ml, 2.30 mmol) was added. The solution was stirred overnight at room temperature, then the solvent was evaporated under vacuum. The product was purified by column chromatography over silica gel using hexane/ethyl acetate as eluent, and concentrated by rotary evaporation to a yellow oil. Yield 22%. R_f = 0.55 (silica gel, 6:4 hexane-ethyl acetate); ^{1}H NMR ($CDCl_3$) δ 8.20 (d, 2H, CH, J = 7.2 Hz), 7.2–7.35 (m, 5H), 7.10 (d, 2H, CH, J = 6.4 Hz), 3.92–3.96 (m, 2H), 2.65–2.75 (m, 1H), 2.39–2.48 (m, 1H), 1.85–2.20 (m, 3H), 1.24–1.80 (m, 8H), 0.8–0.93 (m, 6H); ^{13}C NMR ($CDCl_3$) δ 155.5, 139.3, 139.2, 128.6, 128.2, 125.5, 120.8, 70.5, 39.0, 35.9, 31.0, 29.9, 26.2, 25.1, 22.0, 16.2, 13.8; ^{31}P NMR ($CDCl_3$) δ 31.39, 31.37; MS (CI, NH_3) *m/z* (rel. intensity) 420.0 (5, M + H$^+$), 132 (100, $M^+ - P(O)(C_6H_{13})(OC_6H_4NO_2)OH$), 117 (67, $M^+ - P(O)(C_6H_{13})(OC_6H_4NO_2)OH$ - CH_3), 91 (25, tropylium).

(S_C, R_PS_P) Hexylphosphonic Acid 2-Methyl-3-Phenylpropyl Ester 4-Nitrophenyl Ester, 1-(S)

The reaction was performed as for 1-(*R*). Yield 20% (yellow oil). R_f = 0.55 (silica gel, 6:4 hexane-ethyl acetate); NMR and MS are the same as those for 1-(*R*).

Inactivation of BCL by 1-(*R*) and 1-(*S*)

BCL was dissolved in potassium phosphate buffer (50 mM [pH 7.5]), to a final concentration of 22.5 nM. 1-(*R*) and 1-(*S*) were dissolved in *n*-propanol to a final concentration of 32 mM. The BCL solution (0.25 ml) was mixed with the inactivator solution (0.25 ml) and incubated at room temperature overnight. The hydrolytic activity against *p*-nitrophenol acetate dropped to <2%. The solutions were dialyzed against water for 24 hr. After dialysis, a white precipitate (BCL-inactivator complex) formed. The suspensions were centrifuged at 4300 rpm and 4°C, the supernatant was discarded,

and the protein was redissolved in a solution of 50% *n*-propanol and 50% imidazole buffer (50 mM [pH 6.5]). The complexes were concentrated using Microcon YM-30® ultrafiltration membranes (Millipore Corp., Nepean, Ontario, Canada) and the concentrated protein diluted in the same buffer to a concentration of 10 mg/ml.

Crystallization, Diffraction Data Collection, and Structure Determination for the Complexes BCL-1-(*R*) and BCL-1-(*S*)

Crystals of the complexes were grown by vapor diffusion. The drop contained protein (10 mg/ml) in imidazole buffer (50 mM [pH 6.5], containing 50 vol% *n*-propanol). The reservoir solution contained 50 mM imidazole buffer (pH 6.5), and 25-30 vol% *n*-propanol.

Diffraction data were collected at beamline X8C at the National Synchrotron Light Source, Brookhaven National Laboratory (Upton, NY) using an ADSC (San Diego, CA) Quantum-4 CCD detector. Diffraction data for complex BCL-1-(*R*) were collected at a wavelength of 0.9794 Å in two 180° sweeps. The first sweep was collected with 1° oscillations, 30 s exposures and a crystal to detector distance of 90 mm. The low-resolution reflections that were overloaded in the first sweep were re-collected in a second 180° frame sweep collected at a crystal to detector distance of 140 mm using 4 s exposures. The BCL-1-(*S*) data were collected at a wavelength of 0.9795 Å in 180 frames using 1° oscillations, 60 s exposures, and a distance of 140 mm. Data reduction was performed with DENZO/SCALEPACK [24].

The three-dimensional model of unliganded BCL (PDB ID 3LIP [12],) was placed in the unit cell by rigid body refinement followed by conjugate gradient minimization and simulated annealing refinement using CNS [25]. The model was corrected and solvent was added using 3Fo-2Fc and Fo-Fc difference maps. After conjugate gradient minimization and restrained individual B-factor refinement in CNS, the phosphonate inactivator molecules were modeled into $F_o - F_c$ difference maps. Final refinements were done using Refmac 5.1.24 [26]. The progress of the refinement was monitored by R_{free}, which was calculated from a randomly selected portion (5%) of the diffraction data.

Kinetic Constants for the BCL Catalyzed Hydrolysis of (*R*)- and (*S*)-2-Methyl-3-Phenyl-1-Propyl Heptanoate

k_{cat} and K_M were calculated from kinetic data collected on a SpectraMAX 340 microplate reader using SoftMax Pro 2.2.1 software (Molecular Devices Corp., Sunnyvale, CA) using a *p*-nitrophenol pH indicator to monitor ester hydrolysis. Concentrations in wells were as follows: *N*,*N*-bis-(2-hydroxymethyl)-2-aminoethanesulfonic acid [BES] = 7.55 mM, *p*-nitrophenol [PNP] = 1.25 mM, [BCL] = 2.85 μg/ml or 28.5 μg/ml, [(*R*) and (*S*)-2-methyl-3-phenyl-1-propyl heptanoate] = 0.6 to 4.5 mM, [*n*-propanol] = 27%. Data were analyzed using Eadie-Hofstee plots [27, 28].

Acknowledgments

We thank Dr. Alexandra Weissfloch for initial synthesis of racemic inactivators, the Natural Sciences and Engineering Research Council of Canada (NSERC) for financial support, Dr. Miroslaw Cygler for helpful discussions, and Peter Bernhardt for preparing the PyMol figures. A.M. thanks Les Fonds Québécois de la Recherche sur la Nature et les Technologies for two postgraduate fellowships and Mr. Tobie Généreux-Vincent and Dr. Mohamed Naim for insightful discussions and precious help.

Received: November 26, 2004
Revised: December 30, 2004
Accepted: January 28, 2005
Published: April 21, 2005

References

1. Rouhi, A.M. (2004). Chiral chemistry. Chem. Eng. News *82*, 47–62.
2. Martin, C., Himmele, W., and Siegel, H. (1983). Optically active phenylpropane derivatives, their preparation and their use for the preparation of fungicides. U.S. patent 4410734.
3. Delinck, D.L., and Margolin, A.L. (1990). Synthesis of chiral building blocks for selective adenosine receptor agents. Lipase-catalyzed resolution of 2-benzylpropanol and 2-benzylpropionic acid. Tetrahedron Lett. *31*, 6797–6798.
4. Stoermer, D., Caron, S., and Heathcock, C.H. (1996). Total synthesis of zaragozic acid A (squalestatin S1). Degradation to a relay compound and reassembly of the natural product. J. Org. Chem. *61*, 9115–9125.
5. Bornscheuer, U.T., and Kazlauskas, R.J. (1999). Hydrolases in Organic Synthesis (Weinheim, Germany: Wiley-VCH).
6. Miyazawa, T., Yukawa, T., Koshiba, T., Ueji, S., Yanagihara, R., and Yamada, T. (2001). Enzymatic resolution of 2-phenoxy-1-propanols through the enantioselective acylation mediated by Achromobacter sp. Lipase. Biotechnol. Lett. *23*, 1547–1550.
7. Tuomi, W.V., and Kazlauskas, R.J. (1999). Molecular basis for enantioselectivity of lipase from *Pseudomonas cepacia* toward primary alcohols. Modeling, kinetics, and chemical modification to increase or decrease enantioselectivity. J. Org. Chem. *64*, 2638–2647.
8. Tomić, S., Dobovičnik, V., Šunjić, V., and Kojić-Prodić, B. (2001). Enantioselectivity of *Pseudomonas cepacia* lipase toward 2-methyl-3 (or 4)-arylalkanols: an approach based on the stereoelectronic theory and molecular modeling. Croat. Chem. Acta *74*, 343–357.
9. Zuegg, J., Hönig, H., Schrag, J.D., and Cygler, M. (1997). Selectivity of lipases: conformational analysis of suggested intermediates in ester hydrolysis of chiral primary and secondary alcohols. J. Mol. Cat. B: Enzymatic *3*, 83–98.
10. Cygler, M., Grochulski, P., Kazlauskas, R.J., Schrag, J.D., Bouthillier, F., Rubin, B., Serreqi, A.N., and Gupta, A.K. (1994). A structural basis for the chiral preference of lipases. J. Am. Chem. Soc. *116*, 3180–3186.
11. Zhao, K., and Landry, D.W. (1993). Tetrazole catalyzed synthesis of phosphonate esters. Tetrahedron *49*, 353–368.
12. Schrag, J.D., Li, Y., Cygler, M., Lang, D., Burgdorf, T., Hecht, H.-J., Schmid, R., Schomburg, D., Rydel, T.J., Oliver, J.D., et al. (1997). The open conformation of a *Pseudomonas* lipase. Structure *5*, 187–202.
13. Kovach, I.M., Huhta, D., and Baptist, S. (1991). Active site interactions in hydrated trypsin-organophosphate adducts: a YETI molecular mechanics study. J. Mol. Struct. *226*, 99–110.
14. Lang, D.A., Mannesse, M.L.M., de Haas, G.H., Verheij, H.M., and Dijkstra, B.W. (1998). Structural basis of the chiral selectivity of *Pseudomonas cepacia* lipase. Eur. J. Biochem. *254*, 333–340.
15. Deslongchamps, P., Atlani, P., Fréhel, D., and Malaval, A. (1972). The importance of conformation of the tetrahedral intermediate in the hydrolysis of esters. Selective cleavage of the tetrahedral intermediate controlled by orbital orientation. Can. J. Chem. *50*, 3405–3408.
16. Schulz, T., Pleiss, J., and Schmid, R.D. (2000). Stereoselectivity of *Pseudomonas cepacia* lipase toward secondary alcohols: a quantitative model. Prot. Sci. *9*, 1053–1062.
17. Mezzetti, A., Keith, C., and Kazlauskas, R.J. (2003). Highly enantioselective kinetic resolution of primary alcohols of the type Ph-X-CH(CH_3)-CH_2OH by *Pseudomonas cepacia* lipase: effect of acyl chain length and solvent. Tetrahedron Asymmetry *14*, 3917–3924.
18. Nishizawa, K., Ohgami, Y., Matsuo, N., Kisida, H., and Hirohara, H. (1997). Studies on hydrolysis of chiral, achiral and racemic alcohol esters with *Pseudomonas cepacia* lipase: mechanism of stereospecificity of the enzyme, J. Chem. Soc. Perkin Trans. *2*, 1293–1298.
19. Luić, M., Tomić, S., Leščić, I., Ljubović, E., Šepac, D., Šunjić, V., Vitale, L., Saenger, W., and Kojić-Prodić, B. (2001). Complex of *Burkholderia cepacia* lipase with transition state analog 1-phenoxy-2-acetoxybutane. Eur. J. Biochem. *268*, 3964–3973.
20. Weissfloch, A.N.E., and Kazlauskas, R.J. (1995). Enantiopreference of lipase from *Pseudomonas cepacia* toward primary alcohols. J. Org. Chem. *60*, 6959–6969.
21. Hanson, K.R. (1981). Phenylalanine ammonia-lyase: mirror-image packing of D- and L-phenylalanine and D- and L-transition state analogs into the active site. Arch. Biochem. Biophys. *211*, 575–588.

22. Fersht, A. (1999). Structure and Mechanism in Protein Science (New York: W.H. Freeman and Co.).
23. DeLano, W.L. (2002). The PyMOL Molecular Graphics System (http://www.pymol.org).
24. Otwinowski, Z., and Minor, W. (1997). Processing of x-ray diffraction data collected in oscillation mode. Methods Enzymol. *276*, 307–326.
25. Brünger, A.T., Adams, P.D., Clore, G.C., DeLano, W.L., Gros, P., Grosse-Kunstleve, R.W., Jiang, J.-S., Kuszewski, J., Nilges, M., Pannu, N.S., et al. (1998). Crystallography & NMR system: a new software suite for macromolecular structure determination. Acta Cryst. Sect. D: Biol. Crystallogr. *54*, 905–921.
26. Murshudov, G.N., Lebedev, A., Vagin, A.A., Wilson, K.S., and Dodson, E.J. (1999). Efficient anisotropic refinement of macromolecular structures using FFT. Acta Cryst. Sect. D: Biol. Crystallogr. *55*, 247–255.
27. Eadie, G.S. (1942). The inhibition of cholinesterase by physostigmine and prostigmine. J. Biol. Chem. *146*, 85–93.
28. Hofstee, B.H.J. (1959). Noninverted versus inverted plots in enzyme kinetics. Nature *184*, 1296–1298.
29. Chen, C.-S., Fujimoto, Y., Girdaukas, G., and Sih, C.J. (1982). Quantitative analysis of biochemical kinetic resolutions of enantiomers. J. Am. Chem. Soc. *104*, 7294–7299.
30. Watanabe, A., Yoshimura, T., Mikami, B., Hayashi, H., Kagamiyama, H., and Esaki, N. (2002). Reaction mechanism of alanine racemase from *Bacillus stearothermophilus*. J. Biol. Chem. *277*, 19166–19172.
31. Klaholz, B.P., Mitschler, A., Belema, M., Zusi, C., and Moras, D. (2000). Enantiomer discrimination illustrated by high-resolution crystal structures of the human nuclear receptor hRARγ. Proc. Natl. Acad. Sci. USA *97*, 6322–6327.
32. Cho, J.H., Kim, D.H., Chung, S.J., Ha, N.-C., Oh, B.H., and Yong Choi, K. (2002). Insight into the stereochemistry in the inhibition of carboxypeptidase A with N-(hydroxyaminocarbonyl) phenylalanine: binding modes of an enantiomeric pair of the inhibitor to carboxypeptidase A. Biorg. Med. Chem. *10*, 2015–2022.
33. Stoll, V.S., Eger, B.T., Hynes, R.C., Martichonok, V., Jones, J.B., and Pai, E.F. (1998). Differences in binding modes of enantiomers of 1-acetamido boronic acid based protease inhibitors: crystal structures of γ-chymotrypsin and subtilisin Carlsberg complexes. Biochemistry *37*, 451–462.
34. Petitpas, I., Bhattacharya, A.A., Twine, S., East, M., and Curry, S. (2001). Crystal structure analysis of warfarin binding to human serum albumin. J. Biol. Chem. *276*, 22804–22809.
35. Nonato, M.C., Windom, J., and Clardy, J. (2003). Human methionine aminopeptidase type II in complex with the enantiomers L-methionine and D-methionine (http://pdbbeta.rcsb.org/pdb/explore.do?structureid=1kqo).
36. Vogt, J., Perozzo, R., Pautsch, A., Prota, A., Schelling, P., Pilger, B., Folkers, G., Scapozza, L., and Schulz, G.E. (2000). Nucleoside binding site of herpes simplex type 1 thymidine kinase analyzed by x-ray crystallography. Prot. Struct. Funct. Genet. *41*, 545–553.
37. Cho, H., Ramaswamy, S., and Plapp, B.V. (1997). Flexibility of liver alcohol dehydrogenase in stereoselective binding of 3-butylthiolane 1-oxides. Biochemistry *36*, 382–389.
38. Mesecar, A.D., and Koshland, D.E., Jr. (2000). A new model for protein stereospecificity. Nature *403*, 614–615.
39. Karpusas, M., Holland, D., and Remington, S.J. (1991). 1.9-Å Structures of ternary complexes of citrate synthase with D- and L-malate: mechanistic implications. Biochemistry *30*, 6024–6031.
40. Bone, R., Frank, L., Springer, J.P., Pollack, S.J., Osborne, S.A., Atack, J.R., Knowles, M.R., McAllister, G., Ragan, C.I., Broughton, H.B., et al. (1994). Structural analysis of inositol monophosphatase complexes with substrates. Biochemistry *33*, 9460–9467.
41. Skrzypczak-Jankun, E., Bross, R., Carroll, R.T., Dunham, W.R., and Funk, M.O., Jr. (2001). Three-dimensional structure of a purple lipoxygenase. J. Am. Chem. Soc. *123*, 10814–10820.
42. Raag, R., Li, H., Jones, B.C., and Poulos, T.L. (1993). Inhibitor-induced conformational change in cytochrome P-450CAM. Biochemistry *32*, 4571–4578.
43. Lancaster, C.R.D., and Hartmut, M. (1999). Refined crystal structures of reaction centres from *Rhodopseudomonas viridis* in complexes with the herbicide atrazine and two chiral atrazine derivatives also lead to a new model of the bound carotenoid. J. Mol. Biol. *286*, 883–898.
44. D'Souza, L.J., Gigant, B., Knossow, M., and Green, B.S. (2002). Remarkable remote chiral recognition in a reaction mediated by a catalytic antibody. J. Am. Chem. Soc. *124*, 2114–2115.
45. Ryu, S.-E., Choi, H.-J., and Kim, D.H. (1997). Stereochemistry in inactivation of carboxypeptidase A. Structural analysis of the inactivated carboxypeptidase A by an enantiomeric pair of 2-benzyl-3,4-epoxybutanoic acids. J. Am. Chem. Soc. *119*, 38–41.